Ubide, T., et al., 2021, Volcanic plumbing filters on ocean-island basalt geochemistry: Geology, v. 49, https://doi.org/10.1130/G49224.1

Volcanic plumbing filters on ocean island basalt geochemistry

Teresa Ubide*, Patricia Larrea, Laura Becerril and Carlos Galé
*Correspondence to: t.ubide@uq.edu.au

SUPPLEMENTARY INFORMATION

Petrography and analytical methods

New rock samples were studied macroscopically to select areas of interest for microscopy. Thin sections were prepared by the Servicio General de Apoyo a la Investigación-SAI of the University of Zaragoza (UniZar, Spain), and by the Spanish Geological Survey (IGME-Madrid, Spain). Petrography was undertaken at the Servicio General de Apoyo a la Investigación-SAI (UniZar). Volume fractions of crystals >0.5 mm (dominantly olivine and clinopyroxene, and minor titanomagnetite) were point-counted and proportions cross checked via image analysis of digitised thin sections (Table S2).

Bulk rock chemical analyses of lava flows and feeder dykes were performed at the Spanish Geological Survey Laboratories (IGME-Madrid). Sample beads were prepared by fusion with lithium tetraborate using a PHILIPS PERL'X3 bead maker. Major and selected trace elements were determined on beads by a Panalytical MagiX X-ray fluorescence (XRF) wavelength dispersive spectrometer fitted with an ultrafine Rh anode window X-ray tube. Sodium was analyzed by Atomic Absorption (VARIAN FS-220 Kit) via fusion with lithium metaborate. Relative error on major elements was typically better than ±1.5%. Analytical results are presented together with literature data from El Hierro island in Table S1. For each sample, we provide textural information along with sample coordinates and stratigraphic position. We locate new and literature data on the El Hierro map in Fig. S1.

Modelling crystal accumulation

We calculated accumulation vectors (Table S3) using El Hierro mineral compositions for major elements (olivine in basanite, Gurenko et al., 2009; clinopyroxene in ankaramite, Weis et al., 2015; plagioclase and Cr-titanomagnetite in basanite, Martí et al., 2013; Figs. 2 and S2) and Hawaiian compositions for trace elements (olivine and clinopyroxene in Mauna Kea ankaramite, Jeffries et al., 1995; Fig. S3). Groundmass chemistry was approximated with the whole rock composition of aphyric dyke DAEH4 (basanite with 4.88 wt.% MgO, representative of the ~5 wt.% MgO peak of liquid compositions at El Hierro; Fig. 2). We modelled 20% addition of olivine, clinopyroxene and plagioclase, and 5% addition of titanomagnetite (Figs. 2 and S2).

Least-squares modelling of major elements in porphyritic samples via MINSQ (Herrmann & Berry, 2002; Table S4) used the same mineral compositions as the accumulation vectors. For the liquid composition, we used aphyric dyke DAEH4 as well as aphyric lava LDAEH2 (6.17 wt.% MgO). Restrictions on model abundances were 60 to 100% for groundmass, 0 to 25% for olivine, 0 to 25% for clinopyroxene, 0 to 20% for plagioclase, and 0 to 5% for titanomagnetite. Out of ten porphyritic samples, seven are reproduced as mixtures of aphyric groundmass and volume fractions of crystals matching those observed in the rocks, returning low residuals (Table S4). Minor discrepancies between observed and modelled volume fractions likely relate to variations in the compositions of mineral cargoes and carrier melts, as well as to potential differences between the porphyricity of sample aliquots used to prepare thin sections and those crushed to obtain whole rock analyses.

Modelling fractional crystallisation

We modelled isobaric fractional crystallisation using rhyolite-MELTS v.1.2.0 (Gualda et al., 2012; Table S5, Figs. 2 and S2) from our most MgO-rich aphyric sample (lava LDAEH3; 7.35 wt.% MgO) as a best approximation of the most mafic pre-eruptive melt

composition. We used the NNO oxygen fugacity buffer given the oxidised nature of El Hierro magmas (Longpré et al., 2014, 2017; Taracsák et al., 2019) and a water content of 1 wt.% H_2O, consistent with mean and median H_2O concentrations in olivine- and clinopyroxene-hosted melt inclusions (0.9 and 0.95 wt% H_2O, respectively; Taracsák et al., 2019) and H_2O contents in clinopyroxene crystallised at upper mantle conditions in the western Canary Islands (0.71–1.49 wt% H_2O; Weis et al., 2015). We suppressed crystallisation of orthopyroxene, as it does not occur as a primary phase in El Hierro magmatic products (Carracedo et al., 2001). We selected pressures between 400-700 MPa based on phase equilibria experiments, clinopyroxene-melt barometry and fluid and melt inclusion data (Hansteen and Klügel, 2008; Stroncik et al., 2009; Martí et al., 2013; Longpré et al., 2014, 2017; Klügel et al., 2015; Taracsák et al., 2019), which collectively indicate that the majority of fractionation at El Hierro takes place at upper mantle depths. Our models reproduce the mineral assemblage and compositions at El Hierro, with particular accuracy at 400 MPa (~14 km; the crust-mantle boundary under the island is located at ~12-15 km depth according to geophysical data of Ranero et al., 1995). Models at higher pressures lack olivine (from 600 MPa) and fractionate phases that are not observed (including garnet from 700 MPa).

Thermodynamic modelling results agree with clinopyroxene-melt thermobarometry by Klügel et al. (2015). Their P-T results cluster at 400-700 MPa and 1120-1170 ºC. Within this temperature range, our preferred rhyolite-MELTS model (400 MPa) fractionates the typical phenocryst assemblage at El Hierro (olivine, clinopyroxene and Fe-Ti oxides) with mineral compositions that match those in natural products (Meletlidis et al., 2015) (Table S5). Plagioclase crystallises at lower temperatures and may be enhanced by H_2O loss during magma ascent and degassing (Giacomoni et al., 2014), which at El Hierro is estimated to begin at pressures of at least 300 MPa (Longpré et al., 2017), consistent with the occurrence

of plagioclase mainly as a groundmass phase (Table S2; see also Stroncik et al., 2009). Such constraints suggest relatively direct transport of undegassed magma from deep storage to the surface via dykes (Becerril et al., 2013), with only ephemeral stalling linked to lateral magma transport in the crust (Longré et al., 2014; Klügel et al., 2015). This agrees with our eruptible sweet spot at depths around the crust-mantle boundary (Fig. 4).

To reproduce the decrease of MgO from mantle-derived melts to evolved basaltic melts that dominate OIB plumbing systems, we used two primary compositions reconstituted from high-MgO glasses (as opposed to whole rocks) from Kilauea, Hawaii: 1) tholeiitic primary melt from the most magnesian known picritic glass (Clague et al., 1991); 2) alkaline primary melt from nephelinite glass (A22 of Sisson et al., 2009). Polybaric fractional crystallisation models using rhyolite-MELTS v.1.2.0 (Gualda et al., 2012) from initial pressures of 800 MPa to 2 GPa (~30-80 km depth), down to ~400 MPa, using the NNO oxygen fugacity buffer and water contents between 0.5-1 wt.% H_2O, reproduce the 5 wt.% MgO compositions at El Hierro at mantle depths of ~600 MPa after 50% crystallisation (Table S5; Figs. 2 and S2). The tholeiitic path is relatively enriched in SiO_2 and generates orthopyroxene (not observed at El Hierro), whereas the alkaline path plots above El Hierro data for Na_2O and below for TiO_2. Still, both models produce mineral assemblages and liquid lines of descent that agree with El Hierro data at the 5 wt.% MgO compositional peak. We favour models starting at 800 MPa and considering 1 wt.% H_2O, as they generate fractionating sequences that best fit the observed assemblages at El Hierro. Variations in the physical properties of the melt (density, viscosity, water content) with polybaric (800-400 MPa) fractional crystallisation from the alkaline primary composition are plotted in Fig. 2B.

Additional references

Becerril, L., Galindo, I., and Gudmundsson, A., 2013, Depth of origin of magma in eruptions: Scientific Reports, v. 3, p. 2762, doi:10.1038/srep02762.

Giacomoni, P.P., Ferlito, C., Coltorti, M., Bonadimana, C., and Lanzafame, G., 2014, Plagioclase as archive of magma ascent dynamics on “open conduit” volcanoes: The 2001–2006 eruptive period at Mt. Etna: Earth-Science Reviews, v. 138, p. 371–393.

Guillou, H., Carracedo, J., Torrado, F.P., and Badiola, E.R., 1996, K-Ar ages and magnetic stratigraphy of a hotspot-induced, fast grown oceanic island: El Hierro, Canary Islands: Journal of Volcanology and Geothermal Research, v. 73(1), p. 141–155, doi:10.1016/0377-0273(96)00021-2.

Gurenko, A.A., Sobolev, A.V., Hoernle, K.A., Hauff, F., and Schmincke, H.-U., 2009, Enriched, HIMU-type peridotite and depleted recycled pyroxenite in the Canary plume: A mixed-up mantle: Earth and Planetary Science Letters, v. 277(3), p. 514–524, doi:10.1016/j.epsl.2008.11.013.

Jeffries, T.E., Perkins, W.T., and Pearce, N.J.G., 1995, Measurements of trace elements in basalts and their phenocrysts by laser probe microanalysis inductively coupled plasma mass spectrometry (LPMA-ICP-MS): Chemical Geology, v. 121(1), p. 131–144, doi:10.1016/0009-2541(94)00121-N.

Meletlidis, S., Di Roberto, A., Domínguez Cerdeña, I., Pompilio, M., García-Cañada, L., Bertagnini, A., and Sainz-Maza Aparicio, S., 2015, New insight into the 2011-2012 unrest and eruption of El Hierro Island (Canary Islands) based on integrated geophysical, geodetical and petrological data: Annals of Geophysics, v. 58(5), doi:10.4401/ag-6754.

Weis, F.A., Skogby, H., Troll, V.R., Deegan, F.M., and Dahren, B., 2015, Magmatic water contents determined through clinopyroxene: Examples from the Western Canary Islands, Spain: Geochem. Geophys. Geosyst., v. 16, p. 2127–2146, doi:10.1002/2015GC005800.

Supplementary Figures

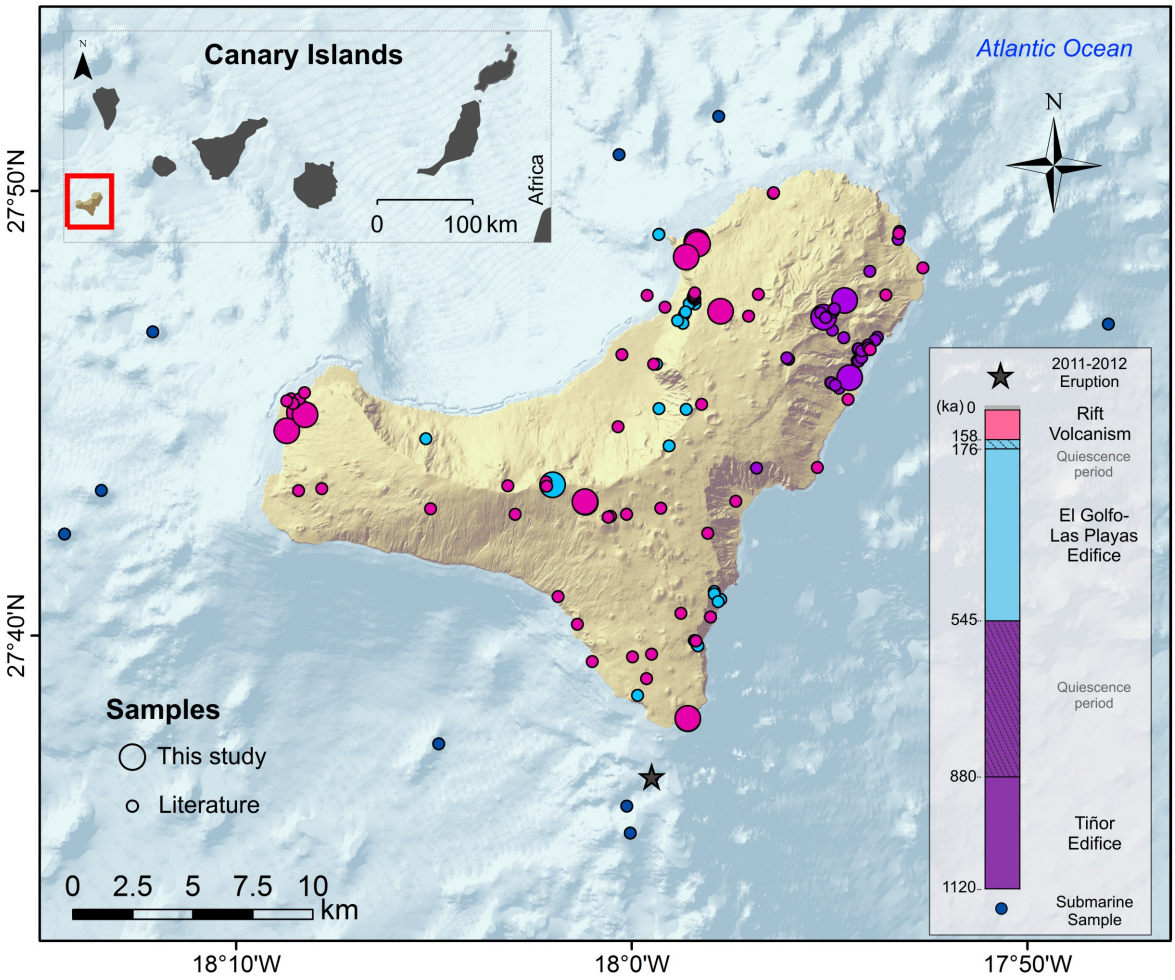

Figure S1. Geological context of samples in our geochemical database (Table S1), colour-coded according to stratigraphy. Submarine samples are shown in dark blue (the location of the 2011-2012 eruption is marked with a star). The map is a digital elevation model of El Hierro, the youngest of the Canary Islands (Spain). The volcano stratigraphy includes three onshore eruptive cycles of shield building subaerial activity since 1.12 Ma (Guillou et al., 1996), separated by periods of quiescence.

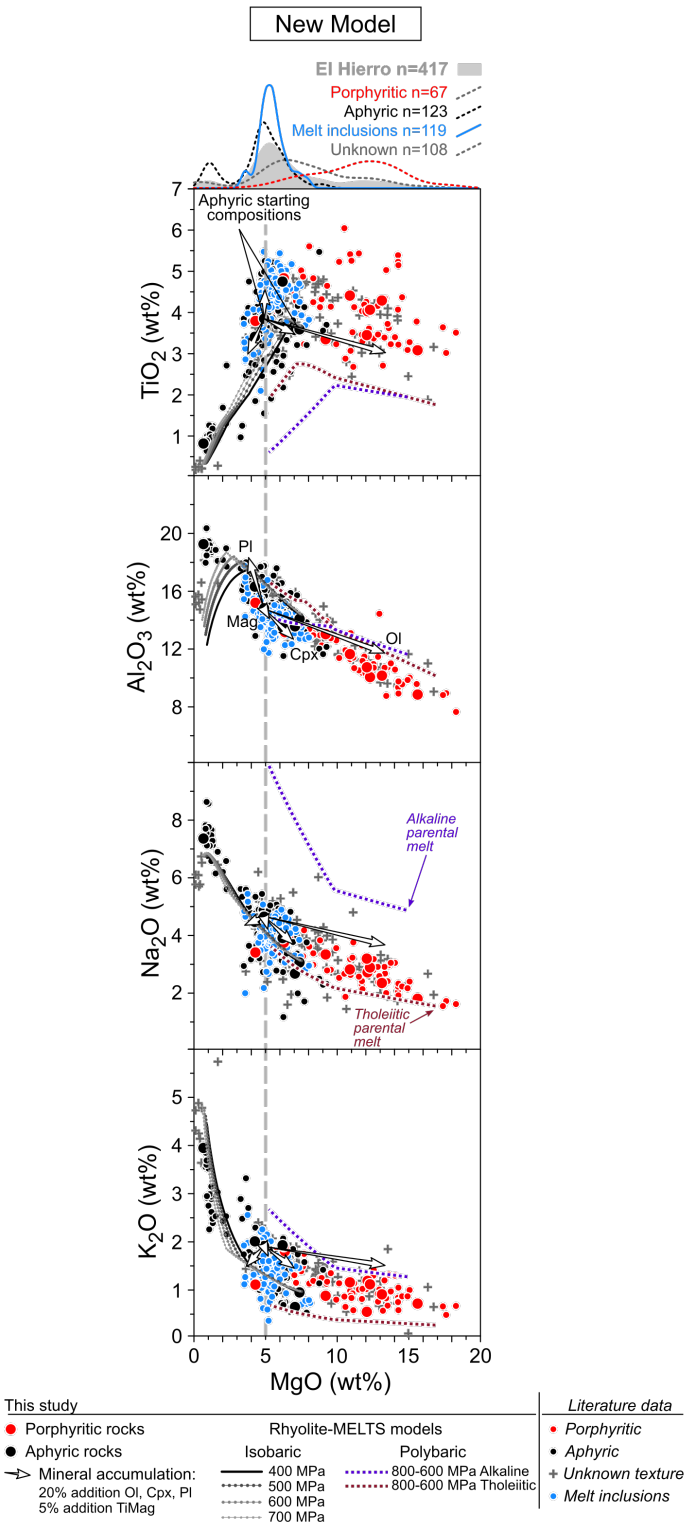

Figure S2. Bivariate diagrams additional to Fig. 2B for El Hierro bulk rocks, glasses and melt inclusions (Table S1), as well as mineral accumulation and rhyolite-MELTS fractional crystallisation models (Tables S3 and S5). Porphyritic mixtures agree with the addition of olivine (Ol), clinopyroxene (Cpx) and minor titanomagnetite (Mag) to an aphyric sample

representative of the main compositional group at 5 wt.% MgO (sample DAEH4), without accumulation of plagioclase (Pl) which is typically restricted to the groundmass. Fractional crystallisation from our least fractionated aphyric sample (7 wt.% MgO; sample LDAEH3) reproduces aphyric data. The 5 wt.% MgO compositional peak results from deep-seated fractional crystallisation of primary melts, starting from Hawaiian liquids reconstituted from glass data (tholeiitic melt from Clague et al., 1991; alkaline melt from Sisson et al., 2009).

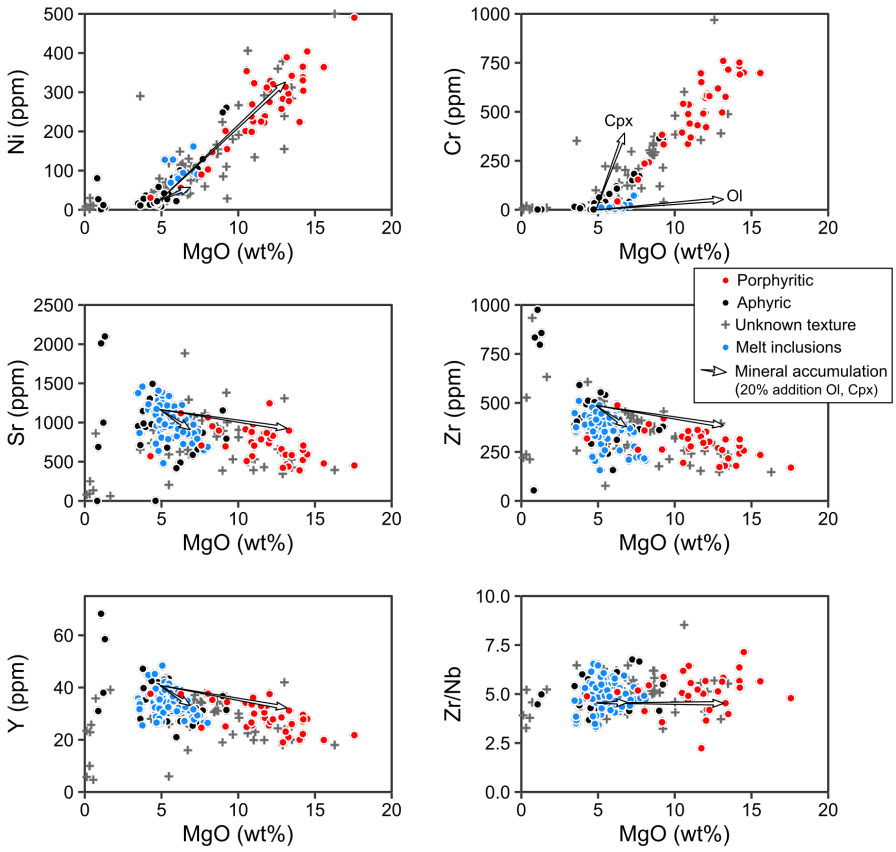

Figure S3. Trace element compositions of bulk rocks, glasses and melt inclusions at El Hierro (Table S1), as well as mineral accumulation vectors (Table S3). Addition of olivine and clinopyroxene to crystal-free melts (Ol and Cpx vectors starting from aphyric sample DAEH4, which has typical ~5 wt.% MgO) reproduces the increase in Cr-Ni associated with the increase of MgO in porphyritic samples, while elements and elemental ratios insensitive to olivine and clinopyroxene (Sr, Y, Zr, Zr/Nb) remain constant.